# Origin of orbital ordering in YTiO<sub>3</sub> and LaTiO<sub>3</sub>

Xue-Jing Zhang,<sup>1</sup> Erik Koch,<sup>1</sup> and Eva Pavarini<sup>1</sup>

<sup>1</sup> Institute for Advanced Simulation, Forschungszentrum Jülich, 52425 Jülich, Germany (Dated: June 16, 2020)

The origin of orbital order in correlated transition-metal compounds is strongly debated. For the paradigmatic  $e_g$  systems KCuF<sub>3</sub> and LaMnO<sub>3</sub>, it has been shown that the electronic Kugel-Khomskii mechanism alone is not sufficient to drive the orbital-ordering transition up to the high temperatures at which it is experimentally observed. In the case of  $t_{2g}$  compounds, however, the role played by the super-exchange interaction remains unclear. Here we investigate this question for two representative systems, the 3d  $t_{2g}^1$  Mott insulators LaTiO<sub>3</sub> and YTiO<sub>3</sub>. We show that the Kugel-Khomskii super-exchange transition temperature,  $T_{\rm KK}$ , is unexpectedly large, comparable to the value for the  $e_g^3$  fluoride KCuF<sub>3</sub>. By deriving the general form of the orbital super-exchange Hamiltonian for the  $t_{2g}^1$  configuration, we show that the GdFeO<sub>3</sub>-type distortion plays a key part in enhancing  $T_{\rm KK}$  to about 300 K. Still, orbital ordering above 300 K can only be ascribed to the presence of a static crystal-field splitting.

### I. INTRODUCTION

Orbital-order in strongly-correlated materials can arise from different types of microscopic mechanisms. The first is the classical Jahn-Teller instability; in this scenario, the electron-lattice coupling produces lattice distortions which remove the orbital degeneracy. crystal-field splitting arising via such distortions can lead to large differences in orbital occupations and regular patterns of mostly occupied orbitals, i.e, to orbital ordering. Remarkably, even if the crystal-field splitting is relatively small in comparison to the bandwidth, the orbital polarization can be large, since it is strongly enhanced by the Coulomb interaction, 2-4 making orbital ordering stable even at very high temperatures. The second mechanism that can lead to orbital ordering phenomena is the electronic super-exchange introduced by Kugel and Khomskii.<sup>5</sup> In this mechanism the ordering arises even in the absence of crystal-field splitting and is due to the orbital super-exchange interaction. The strength of such a purely electronic mechanism has been investigated in detail for the case of the paradigmatic  $e_q$  systems KCuF<sub>3</sub> and LaMnO<sub>3</sub>. It has been shown that the associated transition temperature,  $T_{\rm KK}$ , is too small to explain the presence of orbital ordering well above 1000 K, 4,6-8 as observed experimentally. In the case of KCuF<sub>3</sub> it was shown that even the electron-phonon coupling alone does not explain experimental findings; instead, a new mechanism was identified, in which the Born-Mayer repulsion plays a key role. This new mechanism is in particular relevant for ionic systems. Finally, for layered perovskites yet another mechanism, the orbital super-exchange field, was shown to be at work in addition.<sup>10</sup>

In this complex scenario, it remains yet to be established how strong super-exchange effects are in  $t_{2g}$  materials. Representative systems are the  $3d\,t_{2g}^1$  orthorhombic perovskites LaTiO<sub>3</sub> and YTiO<sub>3</sub>, two strongly-correlated insulators with GdFeO<sub>3</sub>-type structure (see Fig. 1). <sup>12,13</sup> Both compounds are paramagnetic insulators in a wide temperature range. For YTiO<sub>3</sub> the magnetic transition

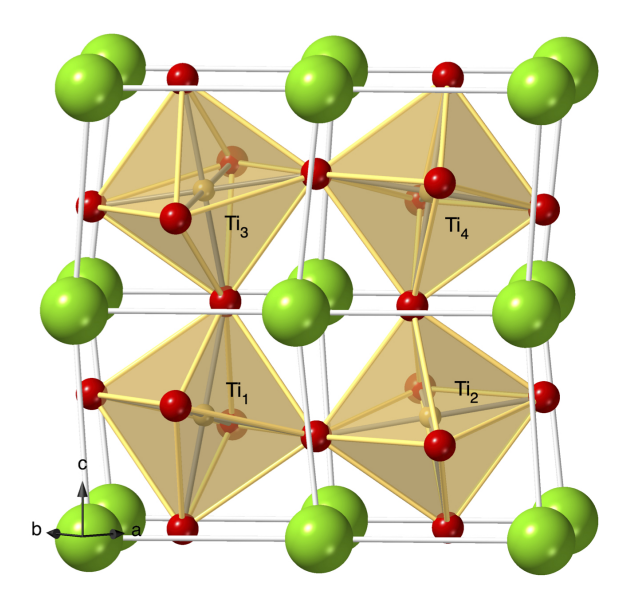


FIG. 1: (Color online) The GdFeO<sub>3</sub>-type perovskite structure<sup>11</sup> of LaTiO<sub>3</sub>. The pseudocubic axes are  $\mathbf{x} \sim (\mathbf{a} + \mathbf{b})/2$ ,  $\mathbf{y} \sim (\mathbf{b} - \mathbf{a})/2$ ,  $\mathbf{z} \sim \mathbf{c}$ . Point symmetry transformations with respect to site Ti<sub>1</sub> are:  $(\hat{x} \leftrightarrow \hat{y})$  for site Ti<sub>2</sub>,  $(\hat{z} \leftrightarrow -\hat{z})$  for site Ti<sub>3</sub> and  $(\hat{x} \leftrightarrow \hat{y}), (\hat{z} \leftrightarrow -\hat{z})$  for site Ti<sub>4</sub>.

temperature to the ferromagnetic ground state is as low as 40 K. Orbital ordering has been detected via various experimental techniques ranging from nuclear magnetic resonance, polarized neutron diffraction, surprise resonance, are polarized neutron diffraction, range magnetic diffraction, for in the polarized neutron diffraction, surprise resonant x-ray scattering, and soft x-ray linear dichroism. For LaTiO<sub>3</sub> the situation is more complex. In  $t_{2g}$  perovskites the gain in super-exchange energy from static Jahn-Teller orbital ordering is expected to be much smaller than in  $e_g$  systems, where orbitals are bond oriented. It was therefore suggested that in LaTiO<sub>3</sub> the proximity to the metal-insulator transition could make the (dynamical) orbital liquid state stable instead. Later, however, evidence in favor of orbital ordering accumulated, as it became clear that, although the Jahn-

Teller distortion is very small, a sizable static crystal-field splitting is generated by the GdFeO<sub>3</sub>-type distortion and the associated deformations of the cubic cation cage.<sup>2,3,22–28</sup> While it is now accepted that LaTiO<sub>3</sub> is orbitally ordered, it still remains to be established what role the super-exchange interaction actually plays in the genesis of such ordering, which, for LaTiO<sub>3</sub> as for YTiO<sub>3</sub>, persists well above the magnetic ordering temperature. This is what we investigate and clarify in this work.

The paper is organized as follows. In Section I we describe the model and method used. The technique we adopt is based on the dynamical mean-field theory (DMFT). It is augmented with the approach we established in Ref. 4 for studying super-exchange driven orbital ordering transitions. In Section II we present the main results. We calculate the order parameter, the orbital polarization p(T), as a function of temperature. We obtain the transition temperature  $T_{\rm KK}$ , which marks the onset of the orbitally ordered phase for the pure super-exchange mechanism, and identify the most occupied natural orbital. We show that in both LaTiO<sub>3</sub> and YTiO<sub>3</sub> the critical temperature  $T_{\rm KK}$  is surprisingly large with respect to some early assumptions. We find  $T_{\rm KK}\sim 300$  K, comparable to the case of the  $e_g^3$  perovskite KCuF<sub>3</sub>. We show that this is mostly due to the GdFeO<sub>3</sub>-type distortion. Remarkably, our results show that the super-exchange interaction alone favors a very similar orbital ordering in YTiO<sub>3</sub> and LaTiO<sub>3</sub>. There is, however, an important difference between the two compounds. In YTiO<sub>3</sub>, where the GdFeO<sub>3</sub>-like distortion is larger, the super-exchange interaction co-operates with the static crystal-field splitting in determining the orbital which is actually occupied; the most occupied natural orbital obtained without crystal-field splitting is very close to the one obtained in the presence of the static crystal-field splitting and observed experimentally. In contrast, for LaTiO<sub>3</sub>, a system

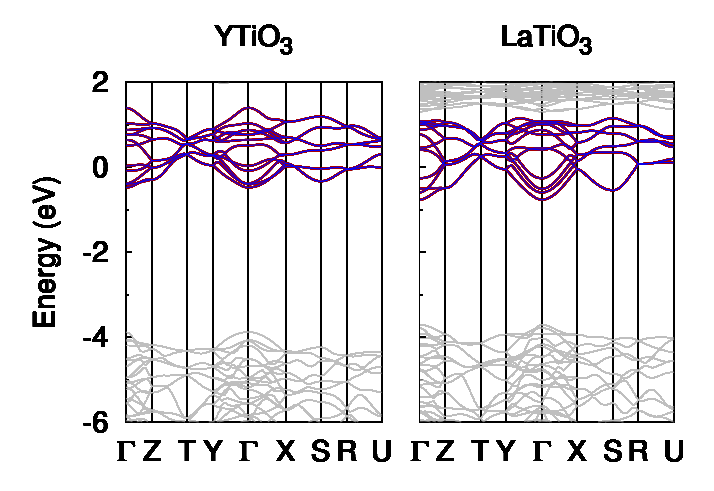


FIG. 2: (Color online) Light gray: LDA band structure of YTiO<sub>3</sub> (left) and LaTiO<sub>3</sub> (right). Dark lines:  $t_{2g}$  bands from the Wannier orbitals, on top of the original LDA bands.

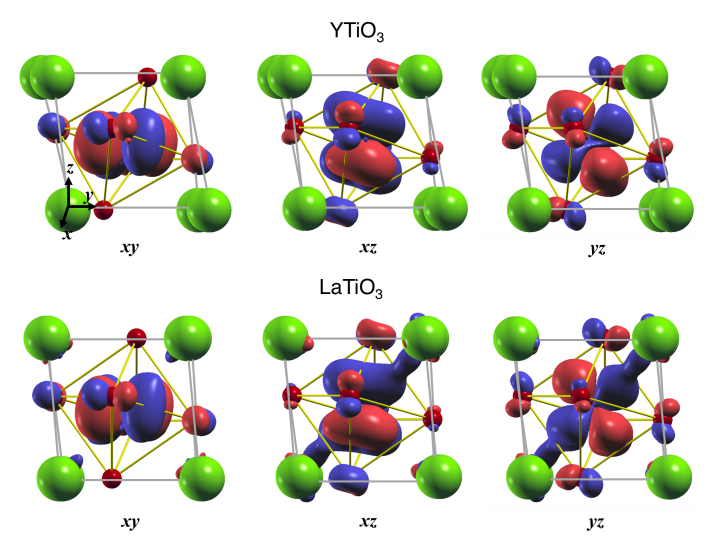


FIG. 3: (Color online) The  $t_{2g}$ -like Wannier basis for YTiO<sub>3</sub> (top) and LaTiO<sub>3</sub> (bottom).

with a much smaller  $GdFeO_3$ -like distortion, it substantially differs, i.e., the super-exchange interaction partially competes with the static crystal-field splitting. The conclusions are summarized in Section III. In the Appendix we present the general orbital super-exchange Hamiltonian for the  $t^1_{2g}$  configuration, used in the discussion presented in Section II.

### II. MODEL AND METHOD

In the first step we perform local density approximation (LDA) calculations using the full-potential linearized augmented plane-wave method as implemented in the WIEN2K code. The LDA bands are shown in Fig. 2. Next we construct localized  $t_{2g}$ -like Wannier functions using projectors and, when needed, the maximal localization procedure. The Wannier orbitals obtained in this way for the experimental structures are shown in Fig. 3. Finally, we build the associated  $t_{2g}$  Hubbard model with full local Coulomb interaction

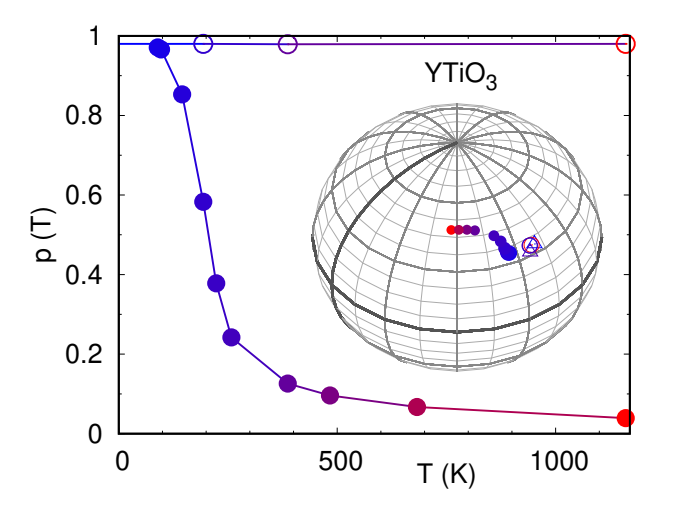
$$\hat{H} = -\sum_{ii'\sigma} \sum_{mm'} t_{mm'}^{i,i'} c_{im\sigma}^{\dagger} c_{im'\sigma} + U \sum_{im} \hat{n}_{im\uparrow} \hat{n}_{im\downarrow}$$

$$+ \frac{1}{2} \sum_{i\sigma\sigma'} \sum_{m \neq m'} (U - 2J - J\delta_{\sigma,\sigma'}) \hat{n}_{im\sigma} \hat{n}_{im'\sigma'}$$

$$- J \sum_{im \neq m'} (c_{im\uparrow}^{\dagger} c_{im\downarrow}^{\dagger} c_{im'\uparrow} c_{im'\downarrow} + c_{im\uparrow}^{\dagger} c_{im\downarrow} c_{im'\downarrow}^{\dagger} c_{im'\uparrow}).$$

$$(1)$$

Here  $t_{mm'}^{i,i'}$  is the LDA hopping integral from orbital m on site i to orbital m' on site i'. The operator  $c_{im\sigma}^{\dagger}$  ( $c_{im\sigma}$ ) creates (annihilates) an electron with spin  $\sigma$  in Wannier state m at site i, and  $n_{im\sigma} = c_{im\sigma}^{\dagger} c_{im\sigma}$ . The parameters U and J are the direct and exchange screened Coulomb interaction; we use U = 5 eV and



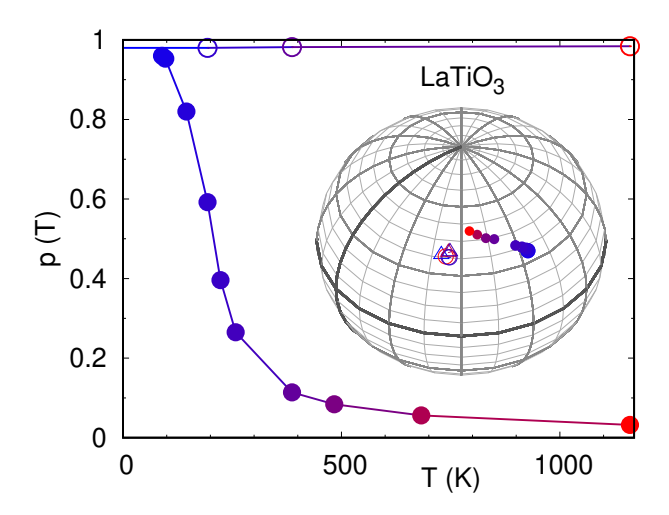


FIG. 4: (Color online) Super-exchange driven orbital-ordering transition in YTiO<sub>3</sub> (left) and LaTiO<sub>3</sub> (right). The figures show the orbital polarization p(T) as a function of temperature. Darker symbols correspond to lower temperatures. For each temperature, the most occupied state,  $|\vartheta,\varphi\rangle_1 = \sin\vartheta\cos\varphi\,|xz\rangle_1 + \cos\vartheta\,|xy\rangle_1 + \sin\vartheta\sin\varphi\,|yz\rangle_1$ , is indicated on the sphere in the inset, where the two dark lines correspond to  $\vartheta = 90^\circ$  (equatorial) and  $\varphi = 0^\circ$  (vertical). Empty circles: LDA+DMFT results with full crystal-field splitting. Filled circles: results in the zero crystal-field splitting limit. Triangles: lowest energy crystal-field orbital from LDA calculations for the experimental structure measured at 2 K and 293 K for YTiO<sub>3</sub> (crystal structures from Refs. 22 and 29), 8 K, 293 K, and 747 K for LaTiO<sub>3</sub> (crystal structures from Refs. 22 and 11).

J=0.64 eV, values which have been established in previous works. 2,3,32 As quantum impurity solver we adopt the generalized hybridization-expansion continuous-time quantum Monte Carlo (CT-HYB QMC) method<sup>33</sup> in the implementation presented in Ref. 8. In order to describe the orbital-ordering transition we adopt the approach we have introduced in Ref. 4 and used with success for several representative  $e_g$  systems.  $^{4,6,7,10}$  To extend this to the case of the  $t_{2g}^1$  configuration we define the orbital polarization (the order parameter) as  $p(T) = n_1 - (n_2 + n_3)/2$ , where  $n_i$  are the occupations of the natural orbitals, ordered such that  $n_i \geq n_{i+1}$ . In the high-temperature para-orbital phase  $p(T) \sim 0$ , while in the  $T \to 0$  limit, i.e., well inside the orbitally ordered phase,  $p(T) \to 1$ . For the experimental structure, we find that the orbital polarization is close to its maximum value already at temperatures as high as 1000 K, and changes little with temperature. In the orbitally ordered phase we identify the most occupied natural orbital at site Ti<sub>1</sub> as the state  $|\vartheta,\varphi\rangle=|\vartheta,\varphi\rangle_1=\sin\vartheta\cos\varphi\,|xz\rangle_1+\cos\vartheta\,|xy\rangle_1+$  $\sin \vartheta \sin \varphi |yz\rangle_1$ . The corresponding occupied orbitals at sites 2, 3, and 4 can be obtained using point-group symmetries:  $|\vartheta,\varphi\rangle_2 = |\vartheta,90^\circ - \varphi\rangle_1$ , while  $|\vartheta,\varphi\rangle_3 = |-\vartheta,\varphi\rangle_1$  and  $|\vartheta,\varphi\rangle_4 = |-\vartheta,90^\circ - \varphi\rangle_1$ . The conclusions so far are in line with established LDA+DMFT results for these materials.  $^{2,3}$ 

In order to extract the transition temperature  $T_{\rm KK}$  for the transition due to super-exchange only, we calculate p(T) for idealized structures. These are obtained by progressively decreasing the effects of the distortions on the on-site energies. We have already shown in the past<sup>4,6–8,10</sup> that this approach reliably determines the upper bound for the critical temperature  $T_{\rm KK}$ , the tempera-

ture which determines the on-set of the super-exchangedriven orbital ordering transition. The results are discussed in the next section.

## III. RESULTS

The main results obtained via LDA+DMFT calculations are shown in Figs. 4 and 5. Let us start from Fig. 4. Here we display the order parameter, p(T), and, on the sphere, the angles  $\vartheta, \varphi$  identifying the most occupied natural orbital,  $|\vartheta,\varphi\rangle$ . These quantities are plotted as a function of temperature, both for YTiO<sub>3</sub> and LaTiO<sub>3</sub>. The figure shows that in the presence of crystalfield splitting (empty circles) orbital-ordering  $p(T) \sim 1$ persists till very high temperatures. This means that, if the structure does not change, no order-to-disorder transition occurs till basically melting temperature. Also, for both systems the most occupied natural orbital,  $|\vartheta,\varphi\rangle$ , is essentially temperature-independent. This can be seen from the positions of the empty symbols on the spheres in Fig. 4. Furthermore  $|\vartheta,\varphi\rangle$  is close to the corresponding lowest energy crystal-field state,  $|\vartheta_{\rm CF}, \varphi_{\rm CF}\rangle$ , shown in the top panels of Fig. 5. The different orbital ordering obtained in the two systems is in good agreement with experiments<sup>39</sup> and can explain also the fact that  $LaTiO_3$ , at low temperatures, orders anti-ferromagnetically, while YTiO<sub>3</sub> ferromagnetically.<sup>3,8</sup> So far, the conclusions are similar to those for  $e_g$  materials.<sup>4,6–8</sup> In order to quantify the strength of the super-exchange interaction, however, we have to analyze the results obtained in the limit of zero crystal-field splitting (filled circles). Fig. 4 shows that the super-exchange transition occurs at  $T_{\rm KK} \sim 300$  K.

This is a remarkably large value given that the titanates are  $t_{2g}$  systems, comparable<sup>4</sup> to the one for the  $e_g$  system KCuF<sub>3</sub> – although still about half the value for the more covalent system  ${\rm LaMnO_3.^{6-8}}$  There is another important result emphasized in the figure. For YTiO<sub>3</sub>, well below the transition temperature  $T_{\rm KK}$ , the most occupied natural orbital  $|\vartheta_{\rm KK}, \varphi_{\rm KK}\rangle$  is identified by the angles  $\vartheta_{\rm KK} \sim 60^\circ$  and  $\varphi_{\rm KK} \sim 90^\circ$ . We therefore obtain  $|\vartheta_{\rm KK}, \varphi_{\rm KK}\rangle \sim |\vartheta_{\rm CF}, \varphi_{\rm CF}\rangle$ ; this can be seen comparing the orbitals shown in the upper and bottom panels of Fig. 5, left column. For LaTiO<sub>3</sub> the situation is quite different; the natural orbital  $|\vartheta_{KK}, \varphi_{KK}\rangle$  is close to the one we find for YTiO<sub>3</sub>, although with a slightly larger  $\varphi_{\rm KK} \sim 100^{\circ}$ . It however differs sizably from  $|\vartheta_{\rm CF}, \varphi_{\rm CF}\rangle$ , with  $\varphi_{\rm CF} \sim 50^{\circ}$ . This can be seen by comparing the orbitals shown in the upper and bottom panels of Fig. 5, right column, or filled and empty symbols on the sphere in Fig. 4, right panel. The state  $|\vartheta_{KK}, \varphi_{KK}\rangle$  also differs from predictions based on super-exchange models for the idealized cubic perovskite structure.  $^{25, \widecheck{27}, 34-36}$  As we will show later, for the ideal cubic structure, the favored orbital in the paramagnetic phase is approximately either  $\frac{1}{\sqrt{3}}|-xz+xy+yz\rangle \sim |55^{\circ},135^{\circ}\rangle$  or one of the states obtained using the (cubic) symmetry transformations:  $(\vartheta, \varphi) \rightarrow (180^{\circ} - \vartheta, \varphi), (\vartheta, \varphi - 180^{\circ})$  and  $(180^{\circ} - \vartheta, \varphi - 180^{\circ}).$ 

In order to better understand these results, we derived the most general super-exchange Hamiltonian for the  $t^1_{2g}$  configuration (paramagnetic phase) and extract its parameters from our LDA+DMFT calculations. To this end, it is convenient to split the super-exchange interaction into its irreducible cubic tensors components

$$\hat{H}_{SE} = \frac{1}{2} \sum_{ij} \hat{H}_{SE}^{ij} = \frac{1}{2} \sum_{ij} \sum_{\mu\mu'} \sum_{r,r'} \hat{\tau}_i^{r,\mu} D_{r\mu,r'\mu'}^{ij} \hat{\tau}_j^{r',\mu'}.$$
(2)

The operator  $\hat{\tau}_i^{r,\mu}$  is the component  $\mu$  of the tensor operator with rank r (in this specific case, r=0,1,2); for convenience we normalize them such that  $\text{Tr}(\hat{\tau}_i^{r,\mu})^2=1$ . The general analytic expression of the Hamiltonian and the super-exchange tensor  $\hat{D}^{ij}$  is given in the Appendix.

In the ideal cubic perovskite case, if one exclusively takes into account the two dominant  $\pi$  bonds, only two orbitals are active in each direction; we define t as the associated hopping integral, identical for all bonds. In this approximation, for two neighboring sites along  $\hat{z}$ , labeled with i and  $j = i \pm \hat{z}$ , the super-exchange Hamiltonian

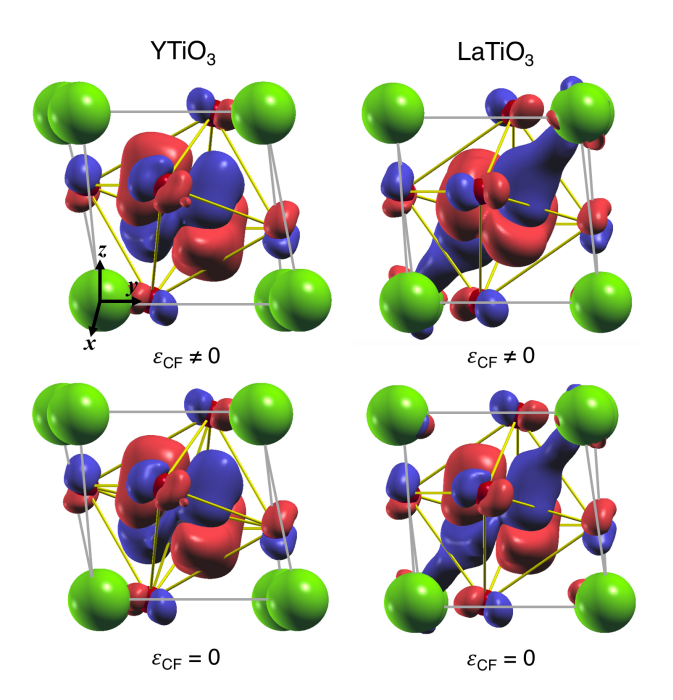


FIG. 5: (Color online) Top: Lowest energy crystal-field orbital at site Ti<sub>1</sub>,  $|\vartheta_{\text{CF}}, \varphi_{\text{CF}}\rangle$ . It is very close to the most occupied natural orbital in the presence of the full static crystal-field splitting  $\varepsilon_{\text{CF}}$ . Bottom: Most occupied natural orbital  $|\vartheta_{\text{KK}}, \varphi_{\text{KK}}\rangle$  for idealized structure with no static crystal-field splitting in the  $T \to 0$  limit. Left: YTiO<sub>3</sub>. Right: LaTiO<sub>3</sub>.

takes the simple form

$$\frac{\hat{H}_{\text{SE}}^{i,j=i\pm\hat{z}}}{2\Gamma_{\text{SE}}} = -\frac{w_1 + 4w_2}{3} \hat{\tau}_i^{0,s} \hat{\tau}_j^{0,s} 
+ \frac{2w_2 - w_1}{2} (\hat{\tau}_i^{1,z} \hat{\tau}_j^{1,z} + \frac{1}{3} \hat{\tau}_i^{2,z^2} \hat{\tau}_j^{2,z^2}) 
- \frac{w_1 + w_2}{3\sqrt{2}} (\hat{\tau}_i^{0,s} \hat{\tau}_j^{2,z^2} + \tau_i^{2,z^2} \hat{\tau}_j^{0,s}) 
+ \frac{w_3 - w_0}{2} \hat{\tau}_i^{2,x^2 - y^2} \hat{\tau}_j^{2,x^2 - y^2} 
+ \frac{w_3 + w_0}{2} \hat{\tau}_i^{2,xy} \hat{\tau}_j^{2,xy},$$
(3)

where  $\Gamma_{\rm SE} = 4t^2/U$  is the energy scale. The parameters  $w_i$  with  $i=0,\ldots,3$  can be expressed in term of the function

$$w(c_1, c_2, c_3) = \frac{c_1}{(1 + 2J/U)} + \frac{c_2}{(1 - J/U)} + \frac{c_3}{(1 - 3J/U)}.$$
(4)

More specifically,  $w_0 = w(\frac{1}{3}, -\frac{1}{3}, 0), w_1 = w(\frac{1}{3}, \frac{2}{3}, 0),$  $w_2 = w(0, \frac{1}{4}, \frac{3}{4}), \text{ and } w_3 = w(0, 0, 1).$  The corresponding Hamiltonian for neighbors along the  $\hat{x}$  direction is

$$\frac{\hat{H}_{\text{SE}}^{i,j=i\pm\hat{x}}}{2\Gamma_{\text{SE}}} = -\frac{w_1 + 4w_2}{3} \hat{\tau}_i^{0,s} \hat{\tau}_j^{0,s} 
+ \frac{2w_2 - w_1}{4} (\hat{\tau}_i^{1,z} \hat{\tau}_j^{1,z} + \frac{5}{3} \hat{\tau}_i^{2,z^2} \hat{\tau}_j^{2,z^2}) 
+ \frac{w_1 + w_2}{6\sqrt{2}} (\hat{\tau}_i^{0,s} \hat{\tau}_j^{2,z^2} + \tau_i^{2,z^2} \hat{\tau}_j^{0,s}) 
+ s \frac{2w_2 - w_1}{4\sqrt{3}} (\hat{\tau}_i^{1,z} \hat{\tau}_j^{2,z^2} + \tau_i^{2,z^2} \hat{\tau}_j^{1,z}) 
- s \frac{w_1 + w_2}{2\sqrt{6}} (\hat{\tau}_i^{0,s} \hat{\tau}_j^{1,z} + \tau_i^{1,z} \hat{\tau}_j^{0,s}) 
+ \frac{w_3 - w_0}{4} (\hat{\tau}_i^{1,x} \hat{\tau}_j^{1,x} + \hat{\tau}_i^{2,xz} \hat{\tau}_j^{2,xz}) 
+ s \frac{w_3 - w_0}{4} (\hat{\tau}_i^{2,xz} \hat{\tau}_j^{1,x} + \hat{\tau}_i^{1,x} \hat{\tau}_j^{2,xz}) 
+ \frac{w_3 + w_0}{4} (\hat{\tau}_i^{1,y} \hat{\tau}_j^{1,y} + \hat{\tau}_i^{2,yz} \hat{\tau}_j^{2,yz}) 
+ s \frac{w_3 + w_0}{4} (\hat{\tau}_i^{1,y} \hat{\tau}_j^{2,yz} + \hat{\tau}_i^{2,yz} \hat{\tau}_j^{1,y}), \quad (5)$$

where s=1. The super-exchange Hamiltonian in  $\hat{y}$  direction  $\hat{H}_{\mathrm{SE}}^{i,j=i\pm\hat{y}}$  can be obtained from the expression for  $\hat{H}_{\mathrm{SE}}^{i,j=i\pm\hat{x}}$  by setting s=-1. In this idealized case, under the local constraint  $n_{xy}+n_{xz}+n_{yz}=1$ , the super-exchange Hamiltonian given above can be recast into a simpler form in terms of spin-1/2 pseudospin operators. For a supercell compatible with the GdFeO<sub>3</sub>-type distortion the associated classical orbitally-ordered ground state is associated with a  $D_{3d}$  octahedral distortion, i.e., approximately the  $\frac{1}{\sqrt{3}}|-xz+xy+yz\rangle$  state. In the formalism just introduced, this type of ordering arises from the terms  $\hat{\tau}_i^{2,xz}\hat{\tau}_j^{2,xz}$  in  $\hat{H}_{\mathrm{SE}}^{i,j=i\pm\hat{x}}$  and  $\hat{H}_{\mathrm{SE}}^{i,j=i\pm\hat{y}}$ .

The general form of the interaction given in Eq. (2) allows us to go from simple models to realistic super-exchange Hamiltonians with general hopping integrals. The full expression for the coupling constants in Eq. (2) can be found in the Appendix.

In Fig. 6 we show  $\Delta E(\vartheta,\varphi)$ , the classical super-exchange energy gain per cell for orbital ordering compatible with the space group of the titanates. It is defined as

$$\Delta E(\vartheta,\varphi) = \frac{1}{N} \sum_{i>i} \left( \langle \Psi_{ij}^{OO} | \hat{H}_{\rm SE}^{ij} | \Psi_{ij}^{OO} \rangle - E_0^{ij} \right)$$
 (6)

where  $|\Psi_{ij}^{OO}\rangle = |\vartheta, \varphi\rangle_i |\vartheta, \varphi\rangle_j$  and the energy zero  $E_0^{ij}$  is the super-exchange energy for the para-orbital state. The terms of Hamiltonian (2) which can give rise to an orbital ordering transition are those which are quadratic in the operators with rank r > 0. The linear terms instead yield an orbital Zeeman effect,<sup>10</sup> and their contributions cancel out in the ideal cubic limit; this can be seen comparing the upper and lower right panels of Fig. 6. The figure also shows that in the cubic perovskite limit the

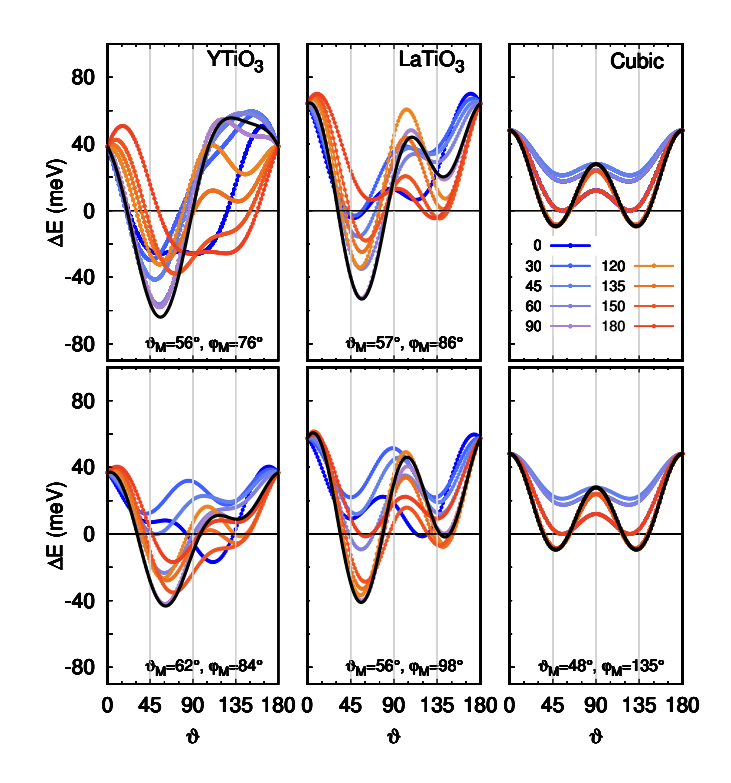


FIG. 6: (Color online) Super-exchange total energy gain  $\Delta E(\vartheta,\varphi)$  for a classical orbitally-ordered ground state compatible with the GdFeO<sub>3</sub>-type distortion. The energy zero is the energy of the para-orbital state. In each panel, the different lines correspond to the values of  $\varphi$  specified in the right top panel. Top panels: all super-exchange terms. Bottom panels: quadratic terms only. Left: YTiO<sub>3</sub>. Center: LaTiO<sub>3</sub>. Right: For comparison, we show the result for the cubic case. We chose  $t \sim 150$  meV, which is a value between the average diagonal hopping integral for LaTiO<sub>3</sub> and YTiO<sub>3</sub>, given in Table I. Black lines:  $\varphi$  values that yield the energy minimum, indicated in each case in the figure. The results are invariant under the transformation  $(\vartheta, \varphi) \to (180^{\circ} - \vartheta, \varphi - 180^{\circ})$ hence we show only results for  $\theta$  and  $\varphi$  between  $0^{\circ}$  and 180°. In the cubic limit an additional symmetry is present,  $(\vartheta, \varphi) \to (180^{\circ} - \vartheta, \varphi).$ 

super-exchange energy gain for a classical orbitally ordered state  $\Delta E(\vartheta, \varphi)$  is, as expected, very small even for the optimal angles. This is because all super-exchange terms but the one arising from  $\hat{\tau}_i^{2,xz}\hat{\tau}_j^{2,xz}$  are either frustrated or cancel out (see Appendix for details) so that

$$\frac{\Delta E(\vartheta,\varphi)}{2\Gamma_{\rm SE}} = \frac{2w_2 - w_1}{24} \left(1 + 3\cos 2\vartheta\right)^2 + \frac{w_3 - w_0}{4} \left(\sin^2 2\vartheta \sin 2\varphi + \frac{1}{4} (1 - \cos 2\vartheta)^2 \sin^2 2\varphi\right).$$
(7)

Furthermore, it has been pointed out that in such a limit quantum fluctuations might even completely prevent ordering at finite temperature.<sup>37</sup> These considerations are completely in line with known results for the pseudo-spin  $1/2 \text{ model.}^{21,22,25,34-36}$ 

In the presence of the GdFeO<sub>3</sub>-type distortion, how-

ever, the hopping integrals couple different orbitals and the simple pseudo-spin-1/2 picture no longer applies in general. Earlier modelizations for the magnetic phase  $^{27,28,34,38}$  have already shown that the GdFeO<sub>3</sub>type distortion can introduce new super-exchange paths, e.g., in a simple tight-binding description, via the coupling of atomic  $e_q$  and  $t_{2q}$  states, thus influencing spinorbital ordering phenomena. Thanks to the general super-exchange Hamiltonian, Eq. (2), and the realistic estimates of the super-exchange parameters obtained in this work via the expressions given in the Appendix, we can now quantify this effect and specify its nature. Furthermore, this can be done specifically for the paramagnetic phase, the one relevant for unraveling the role of the super-exchange interaction in the genesis of orbital ordering at the temperatures where it sets in.

In the left and center panels of Fig. 6 we show  $\Delta E(\vartheta, \varphi)$ for realistic hopping integrals; the values of the latter can be found in Tab. I. The top panels show the total energy gain and the bottom panels the contribution of only the quadratic terms, those that can give rise to a phase transition. The angles  $\vartheta_M, \varphi_M$  that maximize the energy gain, yielding  $\Delta E(\vartheta_M, \varphi_M) = \Delta E_M$ , are basically the same with and without linear terms. Furthermore  $\vartheta_{\rm M}$  and  $\varphi_{\rm M}$  are in accord with  $\vartheta_{\rm KK}$  and  $\varphi_{\rm KK}$  obtained in LDA+DMFT calculations. The energy gain at the optimal angles is  $\Delta E_{\rm M} \sim 40$  meV, also in line with the critical temperature of about  $300~\mathrm{K}$  obtained in LDA+DMFT calculations – taking into account that  $\Delta E_{\rm M}$  is overestimated due to the neglected dynamical quantum effects. This energy gain is about five times larger than the corresponding result in the cubic limit (right panels). By analyzing these results we find that it is the off-diagonal hopping integrals that enhance the super-exchange energy gain, favoring a Jahn-Teller-like natural orbital with  $\varphi_{\rm KK} \sim 90^{\circ}$  over the  $\frac{1}{\sqrt{3}}|-xz+xy+yz\rangle$  natural orbital with  $\varphi_{\rm KK} = 135^{\circ}$ . The super-exchange terms that turn out to contribute most, in addition to  $\hat{\tau}_i^{2,xz}\hat{\tau}_j^{2,xz}$ , are  $\hat{\tau}_j^{1,z}\hat{\tau}_i^{2,xz}$  and  $\hat{\tau}_j^{1,z}\hat{\tau}_j^{1,x}$ , as well as  $\hat{\tau}_i^{2,xz}\hat{\tau}_j^{1,x}$ . This can be understood from Tab. I, which shows the changes in hopping integrals with respect to the cubic limit, and Tabs. II and III which shows the super-exchange tensor elements as a function of the hopping integrals. This conclusion applies to both LaTiO<sub>3</sub> and YTiO<sub>3</sub>, with the angle  $\varphi_{KK}$  slightly smaller than 90° in the case of YTiO<sub>3</sub>, and slightly larger for LaTiO<sub>3</sub>. Figs. 5 and 6, however, also emphasize the main difference between YTiO<sub>3</sub> and LaTiO<sub>3</sub>: while super-exchange effects are rather similar in the two systems, in YTiO<sub>3</sub> they reinforce the effect of the static crystal-field splitting. Instead, in LaTiO<sub>3</sub>, which has a smaller GdFeO<sub>3</sub>-type distortion, they partially compete with it.

Summarizing, in both LaTiO<sub>3</sub> and YTiO<sub>3</sub>, our results show that pure super-exchange effects leading to orbital ordering are much larger than expected from idealized cubic perovskite models. Still, the upper limit for the super-exchange critical temperature, although large, is at most  $T_{\rm KK} \sim 300$  K. Orbital order at higher tem-

|                   |           | YTiO <sub>3</sub> |      |      | $LaTiO_3$ |      |      | cubic |     |     |
|-------------------|-----------|-------------------|------|------|-----------|------|------|-------|-----|-----|
|                   |           |                   | lmn  |      |           | lmn  |      |       | lmn |     |
| $m_1$             | $m'_{i'}$ | 001               | 100  | 010  | 001       | 100  | 010  | 001   | 100 | 010 |
| $\overline{xy_1}$ | $xy_{i'}$ | -5                | -151 | -151 | -16       | -174 | -174 | 0     | -t  | -t  |
| $xz_1$            | $xz_{i'}$ | 162               | -43  | -43  | 198       | -39  | -39  | -t    | 0   | 0   |
| $yz_1$            | $yz_{i'}$ | 46                | 63   | 63   | 180       | 77   | 77   | -t    | 0   | 0   |
| $xy_1$            | $xz_{i'}$ | 82                | -64  | 70   | 51        | -60  | 73   | 0     | 0   | 0   |
| $xz_1$            | $xy_{i'}$ | 82                | 70   | -64  | 51        | 73   | -60  | 0     | 0   | 0   |
| $xy_1$            | $yz_{i'}$ | -66               | -18  | -50  | -61       | -29  | -39  | 0     | 0   | 0   |
| $yz_1$            | $xy_{i'}$ | -66               | -50  | -18  | -61       | -39  | -29  | 0     | 0   | 0   |
| $xz_1$            | $yz_{i'}$ | 73                | 30   | -182 | 52        | 12   | -176 | 0     | 0   | -t  |
| $yz_1$            | $xz_{i'}$ | 73                | -182 | -30  | 52        | -176 | 12   | 0     | -t  | 0   |

TABLE I: Hopping integrals  $-t_{m,m'}^{i,i'}/\text{meV}$  from site i of type  $\text{Ti}_1$  to a site  $i'=i+l\mathbf{x}+m\mathbf{y}+n\mathbf{z}$  of type  $\text{Ti}_2$  or  $\text{Ti}_3$ . From left to right: YTiO<sub>3</sub>, LaTiO<sub>3</sub> and the ideal cubic limit. In the notation adopted, the (xz,yz,xy) Wannier basis changes from site to site due to symmetries. Point symmetry transformations with respect to site  $\text{Ti}_1$  are:  $(\hat{x}\leftrightarrow\hat{y})$  for  $\text{Ti}_2$  and  $(\hat{z}\leftrightarrow-\hat{z})$  for  $\text{Ti}_3$ .

perature can thus only be ascribed to the presence of a static crystal-field splitting. In this respect, a systematic experimental study of the evolution of distortions with increasing temperature well above 300 K would be essential to finally settle the question of the role of superexchange in the genesis of orbital ordering. Some hightemperature data are available for LaTiO<sub>3</sub>. They indicate that all distortions (Jahn-Teller, tilting and rotation angles and the  $D_{3d}$  distortions) either remain unchanged or slightly decrease with increasing temperature. The available structural data have been obtained with different techniques, 11,22,29 and their accuracy might not be directly comparable; nevertheless, based on them, we find that the lowest energy LDA crystal-field orbital does not change much with increasing temperature. The corresponding LDA+DMFT results are shown in Fig. 4. This indicates that orbital ordering stays almost unchanged well above 300 K. If this is experimentally confirmed in both materials, it would show that the super-exchange interaction, although unexpectedly strong, can not drive orbital-order alone in the titanates. This conclusion would then be close to the one we have previously obtained for LaMnO<sub>3</sub> and KCuF<sub>3</sub> and other representative  $e_q$  cases.<sup>4,6–10</sup> It is reinforced by the fact that, while the super-exchange interaction appears to cooperate with crystal-field effects in YTiO<sub>3</sub>, in LaTiO<sub>3</sub> it partially competes with them, while both being orbitally ordered. Finally, the fact that the classical super-exchange energy gain for static orbital ordering is enhanced by about a factor of five in the presence of the GdFeO<sub>3</sub>-type distortion, so that  $T_{KK}$  is, surprisingly, about as large as in KCuF<sub>3</sub>, supports the view that processes involving dynamical orbital fluctuations are not likely to play a role in determining the orbital physics of either system.

#### IV. CONCLUSIONS

We have studied the role of super-exchange in the origin of orbital ordering in representative  $t_{2q}$  materials, YTiO<sub>3</sub> and LaTiO<sub>3</sub>. We adopted an approach that we have previously established and successfully used for  $e_q$  systems.<sup>4,6–8</sup> We find that the super-exchange transition temperature is, surprisingly, as large as in the case of KCuF<sub>3</sub>, a paradigmatic  $e_q$  orbitally-ordered material. We show it is strongly enhanced by the GdFeO<sub>3</sub>-type distortion. While in the case of YTiO<sub>3</sub> the super-exchange most occupied orbital  $|\vartheta_{\rm KK}, \varphi_{\rm KK}\rangle$  is similar to the lowest energy crystal-field state  $|\vartheta_{\rm CF}, \varphi_{\rm CF}\rangle$ , in LaTiO<sub>3</sub> they differ substantially. This indicates that in YTiO<sub>3</sub> lattice distortions reinforce super-exchange effects, while in the case of LaTiO<sub>3</sub> the two effects compete. High temperature structural data are to the best of our knowledge only available for LaTiO<sub>3</sub> so far. They indicate no substantial change in the occupied orbital up to 700 K, i.e., well above  $T_{KK}$ . Orbital ordering persisting till that temperature cannot be explained by the super-exchange mechanism alone, and needs the explicit presence of a static crystal-field splitting. This conclusion is reinforced by fact that in LaTiO<sub>3</sub> the super-exchange most occupied natural orbital differs substantially from the experimental one.

# Appendix: Orbital super-exchange for $t_{2g}^1$ systems

Here we give the general form of the super-exchange interaction, expressed as a function of orbital irreducible cubic tensor operators  $\hat{\tau}_i^{r,\mu}$  of rank r=0,1,2, with components  $\mu=-r,...,r$ 

$$\hat{H}_{SE} = \frac{1}{2} \sum_{ij} \sum_{\mu\mu'} \sum_{rr'} \hat{\tau}_i^{r,\mu} D_{r\mu,r'\mu'}^{ij} \hat{\tau}_j^{r'\mu'}.$$
 (A.1)

We obtain the super-exchange Hamiltonian from secondorder perturbation theory and project it into its irreducible tensor components. For convenience we chose the normalization of the tensor operators such that  $\text{Tr}(\hat{\tau}_i^{r,\mu})^2 = 1$  and split the expression of the tensor elements appearing in Eq. (A.1) in two terms,

$$D^{ij}_{r\mu,r'\mu'} = B^{ij}_{r\mu,r'\mu'} + C^{ij}_{r\mu,r'\mu'}. \tag{A.2} \label{eq:A.2}$$

The first term is

$$B_{r\mu,r'\mu'}^{ij} = -2\sum_{abcd} \langle a|\hat{\tau}_{i}^{r,\mu}|c\rangle\langle b|\hat{\tau}_{j}^{r'\mu'}|d\rangle \frac{t_{c,d}^{i,j}}{U} \frac{t_{a,b}^{i,j}}{U}$$

$$\left[ w_{1}(\delta_{\mu',0} + \delta_{\mu,0}) + w_{0}(2 - \delta_{\mu',0} - \delta_{\mu,0}) \right],$$
(A.3)

and the second

$$\begin{split} C^{ij}_{r\mu,r'\mu'} &= -4 \sum_{acbd} \langle a | \hat{\tau}^{r,\mu}_i | c \rangle \langle d | \hat{\tau}^{r',\mu'}_j | b \rangle \\ & \left[ w_2 \sum_{m_1} \left( \delta_{\mu'r',0s} \frac{t^{i,j}_{c,m_1} \overline{t^{i,j}_{a,m_1}}}{U} + \delta_{\mu r,0s} \frac{\overline{t^{i,j}_{m_1,b}} t^{i,j}_{m_1,d}}{U} \right) \right. \\ & \left. - \frac{t^{i,j}_{c,d} \overline{t^{i,j}_{a,b}}}{U} \left( w_2 (\delta_{\mu',0} + \delta_{\mu,0}) + \frac{w_3}{2} (2 - \delta_{\mu,0} - \delta_{\mu',0}) \right) \right], \end{split}$$

where a, b, c, d are  $t_{2g}$  states. The parameters  $w_i$  with i = 0, ..., 3 can be expressed as  $w_0 = w(\frac{1}{3}, -\frac{1}{3}, 0), w_1 = w(\frac{1}{3}, \frac{2}{3}, 0), w_2 = w(0, \frac{1}{4}, \frac{3}{4})$  and  $w_3 = w(0, 0, 1)$ , where

$$w(c_1, c_2, c_3) = \frac{c_1}{1 + 2J/U} + \frac{c_2}{1 - J/U} + \frac{c_3}{1 - 3J/U}.$$
 (A.5)

In the special case of diagonal hopping integrals the only terms which are non zero are those given in Tab. II. For bonds in  $\hat{x}$  direction we thus have for  $j=i\pm\hat{x}$ 

$$\begin{split} \hat{H}_{\mathrm{SE}}^{i,j} &= -\frac{4(t_{xz,xz}^2 + t_{xy,xy}^2)}{U} \frac{w_1 + 4w_2}{3} \hat{\tau}_i^{0,s} \hat{\tau}_j^{0,s} \\ &+ \frac{4t_{xz,xz}^2}{U} \frac{2w_2 - w_1}{2} \hat{\tau}_i^{1,z} \hat{\tau}_j^{1,z} \\ &+ \frac{4(t_{xz,xz}^2 + 4t_{xy,xy}^2)}{U} \frac{2w_2 - w_1}{6} \hat{\tau}_i^{2,z^2} \hat{\tau}_j^{2,z^2} \\ &+ \frac{4(2t_{xy,xy}^2 - t_{xz,xz}^2)}{U} \frac{w_1 + w_2}{3\sqrt{2}} \left( \hat{\tau}_i^{0,s} \hat{\tau}_j^{2,z^2} + \tau_i^{2,z^2} \hat{\tau}_j^{0,s} \right) \\ &+ s_x \frac{2t_{xz,xz}^2}{U} \frac{2w_2 - w_1}{\sqrt{3}} \left( \hat{\tau}_i^{1,z} \hat{\tau}_j^{2,z^2} + \tau_i^{2,z^2} \hat{\tau}_j^{1,z} \right) \\ &- s_x \frac{4t_{xz,xz}}{U} \frac{w_1 + w_2}{\sqrt{6}} \left( \hat{\tau}_i^{0,s} \hat{\tau}_j^{1,z} + \tau_i^{1,z} \hat{\tau}_j^{0,s} \right) \\ &+ \frac{4t_{xz,xz}t_{xy,xy}}{U} \frac{w_3 - w_0}{2} \left( \hat{\tau}_i^{1,x} \hat{\tau}_j^{1,x} + \hat{\tau}_i^{2,xz} \hat{\tau}_j^{2,xz} \right) \\ &+ s_x \frac{4t_{xz,xz}t_{xy,xy}}{U} \frac{w_3 - w_0}{2} \left( \hat{\tau}_i^{2,xz} \hat{\tau}_j^{1,x} + \hat{\tau}_i^{1,x} \hat{\tau}_j^{2,xz} \right) \\ &+ \frac{4t_{xz,xz}t_{xy,xy}}{U} \frac{w_3 + w_0}{2} \left( \hat{\tau}_i^{1,y} \hat{\tau}_j^{1,y} + \hat{\tau}_i^{2,yz} \hat{\tau}_j^{2,yz} \right) \\ &+ s_x \frac{4t_{xz,xz}t_{xy,xy}}{U} \frac{w_3 + w_0}{2} \left( \hat{\tau}_i^{1,y} \hat{\tau}_j^{2,yz} + \hat{\tau}_i^{2,yz} \hat{\tau}_j^{2,yz} \right) \right), \end{split}$$

where  $s_x=1$ . The super-exchange Hamiltonian  $H_{\rm SE}^{i,j=i\pm\hat{y}}$  can be obtained using symmetries, i.e., by exchanging in the prefactors  $x\leftrightarrow y$  and setting  $s_y=-s_x$ . Next we define  $p_{r,\mu}={}_i\langle\vartheta,\varphi|\hat{\tau}_i^{r,\mu}|\vartheta,\varphi\rangle_i$ . The relevant non-zero terms are, for i corresponding to site Ti<sub>1</sub> (see Fig. 1)

$$p_{1,z} = (1 - \cos 2\theta) \cos 2\phi / 2\sqrt{2}$$
 (A.7)

$$p_{1,x} = \sin 2\theta (\cos \varphi + \sin \varphi)/2,$$
 (A.8)

$$p_{2,z^2} = -(1+3\cos 2\theta)/2\sqrt{6},$$
 (A.9)

$$p_{2,xz} = \sin 2\theta (\cos \varphi - \sin \varphi)/2,$$
 (A.10)

$$p_{2,x^2-y^2} = (1 - \cos 2\theta) \sin 2\varphi / 2\sqrt{2}.$$
 (A.11)

If only diagonal hopping integrals are present, the classical energy associated with orbital order compatible with

| $r \mu$     | $r' \mu'$         | $D^{ij}_{r\mu,r'\mu'}$   | $r \mu r' \mu$   | $\left  D^{ij}_{r\mu,r'\mu'}  ight $   |
|-------------|-------------------|--|--|--|
|             |                   |  |  |  |
| $0 \ s$     | $0 \ s$           | $ -\frac{4}{U} \frac{w_1 + 4w_2}{3} (t_{xz,xz}^2 + t_{yz,yz}^2 + t_{xy,xy}^2) $            | 1z $1z$  | $+\frac{4}{U}\frac{2w_2-w_1}{2}(t_{xz,xz}^2+t_{yz,yz}^2)$  |
| $2 z^2$     | $2 z^2$           | $+\frac{4}{U}\frac{2w_2-w_1}{6}\left(t_{xz,xz}^2+t_{yz,yz}^2+4t_{xy,xy}^2\right)$          | 0 s 1 z  | $-\frac{4}{U}\frac{w_1+w_2}{\sqrt{6}}$ $(t_{xz,xz}^2-t_{yz,yz}^2)$                               |
| $0 \ s$     | $2 z^2$           | $ -\frac{4}{U} \frac{w_1 + w_2}{3\sqrt{2}}  (t_{xz,xz}^2 + t_{yz,yz}^2 - 2t_{xy,xy}^2) $   | $1 z 	 2 z^2$  | $+\frac{4}{U}\frac{2w_2-w_1}{2\sqrt{3}}\left(t_{xz,xz}^2-t_{yz,yz}^2\right)$                     |
| 1 x         | 1 x               | $\left  +\frac{4}{U} \frac{w_3-w_0}{2} \right  \left(t_{xz,xz}+t_{yz,yz}\right) t_{xy,xy}$ | $\begin{array}{ c c c c c c c c c c c c c c c c c c c$ | $+\frac{4}{U}\frac{w_0+w_3}{2} (t_{xz,xz}+t_{yz,yz})t_{xy,xy}$                                   |
| $2 \ xz$    | $2 \ xz$          | $\left  +\frac{4}{U} \frac{w_3-w_0}{2} \right  \left(t_{xz,xz}+t_{yz,yz}\right) t_{xy,xy}$ | $\begin{array}{c ccccccccccccccccccccccccccccccccccc$  | $+\frac{4}{U}\frac{w_0+w_3}{2} (t_{xz,xz}+t_{yz,yz})t_{xy,xy}$                                   |
| $2 x^2 - y$ | $x^2 2 x^2 - y^2$ | $ + \frac{8}{U} \frac{w_3 - w_0}{2}  t_{xz,xz} t_{yz,yz} $                                 | $\begin{array}{ c c c c c c c c c c c c c c c c c c c$ | $\left  +\frac{8}{U} \frac{w_0+w_3}{2} \right  t_{xz,xz} t_{yz,yz}$                              |
| 1 x         | $2 \ xz$          | $\left  +\frac{4}{U} \frac{w_3 - w_0}{2} \right  (t_{xz,xz} - t_{yz,yz}) t_{xy,xy}$        | $\begin{vmatrix} 1 & y & 2 & xz \end{vmatrix}$         | $\left  +\frac{4}{U} \frac{w_0 + w_3}{2} \right  \left( t_{xz,xz} - t_{yz,yz} \right) t_{xy,xy}$ |

TABLE II: Tensor elements different from zero in the case in which the hopping integrals are only diagonal.

| $r \mu$     | $r' \; \mu'$          | $D^{ij}_{r\mu,r'\mu'}$                                   |   |
|-------------|-----------------------|--|---|
|             |                       |  |   |
| 1 z         | 1 z                   | $-\frac{4}{U}\frac{2w_2-w_1}{2}$                         | $(t_{xz,yz}^2 + t_{yz,xz}^2)$   |
| 1 z         | $2 z^2$               | $+\frac{4}{U}\frac{2w_2-w_1}{2\sqrt{3}}$                 | $(t_{xz,yz}^2 - t_{yz,xz}^2 - 2(t_{xz,xy}^2 - t_{yz,xy}^2))$  |
| $2 z^2$     | $2 z^2$               | $+\frac{4}{U}\frac{2w_2-w_1}{6}$                         | $(t_{xz,yz}^2+t_{yz,xz}^2-2(t_{xz,xy}^2+t_{xy,xz}^2+t_{yz,xy}^2+t_{xy,yz}^2)+4t_{xy,xy}^2)$                 |
| 1 z         | 1 x                   | $+\frac{4}{U}\frac{2w_2+w_3-w_1-w_0}{2\sqrt{2}}$         | $((t_{xz,xz} + t_{xz,yz})t_{xz,xy} - (t_{yz,xz} + t_{yz,yz})t_{yz,xy})$                                     |
| 1 z         | $2 \ xz$              | $+\frac{4}{U}\frac{2w_2+w_3-w_1-w_0}{2\sqrt{2}}$         | $((t_{xz,xz}-t_{xz,yz})t_{xz,xy}-(t_{yz,xz}-t_{yz,yz})t_{yz,xy})$   |
| 1 z         | $2 x^2 - y^2$         | $+\frac{4}{U}\frac{2w_2+w_3-w_1-w_0}{2}$                 | $(t_{xz,xz}t_{xz,yz}-t_{yz,xz}t_{yz,yz})$   |
| $2 z^2$     | 1 x                   | $+\frac{4}{U}\frac{2w_2+w_3-w_1-w_0}{2\sqrt{6}}$         | $((t_{xz,xz}+t_{xz,yz})t_{xz,xy}+(t_{yz,xz}+t_{yz,yz})t_{yz,xy}-2(t_{xy,xz}+t_{xy,yz})t_{xy,xy})$           |
| $2z,^2$     | 2 xz                  | $+\frac{4}{U}\frac{2w_2+w_3-w_1-w_0}{2\sqrt{6}}$         | $((t_{xz,xz} - t_{xz,yz})t_{xz,xy} + (t_{yz,xz} - t_{yz,yz})t_{yz,xy} - 2(t_{xy,xz} - t_{xy,yz})t_{xy,xy})$ |
| $2 z^2$     | $2 x^2 - y^2$         | $+\frac{4}{U}\frac{2w_2+w_3-w_1-w_0}{2\sqrt{3}}$         | $(t_{xz,xz}t_{xz,yz} + t_{yz,xz}t_{yz,yz} - 2t_{xy,xz}t_{xy,yz})$   |
| 1 x         | 1 x                   | $+\frac{4}{U}\frac{w_3-w_0}{2}$                          | $((t_{xz,yz} + t_{yz,xz})t_{xy,xy} + (t_{xz,xy} + t_{yz,xy})(t_{xy,xz} + t_{xy,yz}))$                       |
| 1 x         | 2 xz                  | $+\frac{4}{U}\frac{w_3-w_0}{2}$                          | $((-t_{xz,yz}+t_{yz,xz})t_{xy,xy}+(t_{xz,xy}+t_{yz,xy})(t_{xy,xz}-t_{xy,yz}))$                              |
| 2 xz        | 2 xz                  | $-\frac{4}{U}\frac{w_3-w_0}{2}$                          | $((t_{xz,yz} + t_{yz,xz})t_{xy,xy} - (t_{xz,xy} - t_{yz,xy})(t_{xy,xz} - t_{xy,yz}))$                       |
| $2 x^2 - y$ | $y^2 \ 2 \ x^2 - y^2$ | $+\frac{8}{U}\frac{w_3-w_0}{2}$                          | $t_{xz,yz}t_{yz,xz}$  |
| 1 x         | $2 x^2 - y^2$         | $+\frac{8}{U}\frac{w_3-w_0}{2\sqrt{2}}$                  | $((t_{xz,xz} + t_{yz,xz})t_{xy,yz} + (t_{xz,yz} + t_{yz,yz})t_{xy,xz})$                                     |
| 2 xz        | $2 x^2 - y^2$         | $+\frac{8}{U}\frac{w_3-w_0}{2\sqrt{2}}$                  | $((t_{xz,xz}-t_{yz,xz})t_{xy,yz}+(t_{xz,yz}-t_{yz,yz})t_{xy,xz})$   |
|             |                       |  |   |
| $0 \ s$     | 1 x                   | $-\frac{4}{U}\frac{4w_2-w_3+w_1+w_0}{2\sqrt{3}}$         | $((t_{xz,xz} + t_{xz,yz})t_{xz,xy} + (t_{yz,xz} + t_{yz,yz})t_{yz,xy} + (t_{xy,xz} + t_{xy,yz})t_{xy,xy})$  |
| $0 \ s$     | 1 z                   | $-\frac{4}{U}\frac{w_1+w_2}{\sqrt{6}}$                   | $(t_{yz,xz}^2 + t_{xy,xz}^2 - t_{xz,yz}^2 - t_{xy,yz}^2)$   |
| $0 \ s$     | $2 \ xz$              | $-\frac{4}{U}\frac{4w_2 - w_3 + w_1 + w_0}{2\sqrt{3}}$   | $((t_{xz,xz} - t_{xz,yz})t_{xz,xy} + (t_{yz,xz} - t_{yz,yz})t_{yz,xy} + (t_{xy,xz} - t_{xy,yz})t_{xy,xy})$  |
| $0 \ s$     | $2 x^2 - y^2$         | $ -\frac{4}{U} \frac{4w_2 - w_3 + w_1 + w_0}{\sqrt{6}} $ | $(t_{xz,xz}t_{xz,yz} + t_{yz,xz}t_{yz,yz} + t_{xy,xz}t_{xy,yz})$  |
| $0 \ s$     | $2 z^2$               | $-\frac{4}{U}\frac{w_1+w_2}{3\sqrt{2}}$                  | $(t_{yz,xz}^2 + t_{xy,xz}^2 + t_{xz,yz}^2 + t_{xy,yz}^2 - 2t_{xz,xy}^2 - 2t_{yz,xy}^2)$                     |

TABLE III: Additional quadratic  $(r \neq 0, r' \neq 0)$  and linear terms  $(r = 0, r' \neq 0)$  present if the off-diagonal hopping integrals are non zero. Only relevant contributions are listed; in the table we assume for simplicity that the hopping integrals are real, as in the case considered in this paper.

the space group of the titanates is thus  $\Delta E(\vartheta, \varphi) = \Delta E_Q(\vartheta, \varphi) + \Delta E_L(\vartheta, \varphi)$ , where the quadratic term is

$$\begin{split} \Delta E_Q(\vartheta,\varphi) &= \frac{4(t_{xz,xz}^2 + t_{yz,yz}^2 + 4t_{xy,xy}^2)}{U} \frac{2w_2 - w_1}{3} \ p_{2,z^2}^2 \\ &\quad + \frac{4(t_{xz,xz} + t_{yz,yz})t_{xy,xy}}{U} \frac{w_3 - w_0}{2} (p_{1,x}^2 - p_{2,xz}^2) \\ &\quad + \frac{8t_{xz,xz}t_{yz,yz}}{U} \frac{w_3 - w_0}{2} p_{2,x^2 - y^2}^2 \\ &\quad - \frac{4(t_{xz,xz}^2 - t_{yz,yz}^2)}{U} \frac{2w_2 - w_1}{\sqrt{3}} p_{1,z}p_{2,z^2} \\ &\quad + \frac{8(t_{xz,xz} - t_{yz,yz})t_{xy,xy}}{U} \frac{w_3 + w_0}{2} p_{1,x}p_{2,xz} \end{split}$$

and the linear term is

$$\begin{split} \Delta E_L(\vartheta,\varphi) &= -\frac{16(t_{xz,xz}^2 + t_{yz,yz}^2 - 2t_{xy,xy}^2)}{U} \frac{w_1 + w_2}{3\sqrt{6}} p_{2,z^2} \\ &\quad + \frac{8(t_{xz,xz}^2 - t_{yz,yz}^2)}{U} \frac{w_1 + w_2}{\sqrt{18}} p_{1,z}. \end{split} \tag{A.13}$$

In the cubic limit, in which all non-zero hopping integrals are identical, all linear and some of the quadratic terms cancel and this further simplifies to

$$\frac{\Delta E(\vartheta,\varphi)}{2\Gamma_{\text{SE}}} = (2w_2 - w_1)p_{2,z^2}^2 + \frac{w_3 - w_0}{2} \left(p_{1,x}^2 - p_{2,xz}^2 + p_{2,x^2 - y^2}^2\right),$$
(A.14)

where  $\Gamma_{\rm SE} = \frac{4t^2}{U}$ . Hence, in this case, only the  $\hat{\tau}^i_{2xz}\hat{\tau}^j_{2xz}$  term yields an actual energy gain.

- <sup>1</sup> J. Kanamori, J. Appl. Phys. **31**, S14 (1960).
- <sup>2</sup> E. Pavarini, S. Biermann, A. Poteryaev, A.I. Lichtenstein, A. Georges, O.K. Andersen, Phys. Rev. Lett. **92**, 176403 (2004).
- <sup>3</sup> E. Pavarini, A. Yamasaki, J. Nuss, and O.K. Andersen, New J. Phys. 7, 188 (2005).
- <sup>4</sup> E. Pavarini, E. Koch, A.I. Lichtenstein, Phys. Rev. Lett. 101, 266405 (2008).
- <sup>5</sup> K. I. Kugel' and D. I. Khomskii, Zh. Eksp. Teor. Fiz. **64**, 1429 (1973) [Sov. Phys. JETP **37**, 725 (1973)].
- <sup>6</sup> E. Pavarini and E. Koch, Phys. Rev. Lett. **104**, 086402 (2010).
- A. Flesch, G. Zhang, E. Koch, and E. Pavarini, Phys. Rev. B 85, 035124 (2012).
- <sup>8</sup> A. Flesch, E. Gorelov, E. Koch, and E. Pavarini, Phys. Rev. B 87, 195141 (2013).
- <sup>9</sup> H. Sims, E. Pavarini, and E. Koch, Phys. Rev. B **96**, 054107 (2017)
- <sup>10</sup> J. Musshoff, G. Zhang, E. Koch, and E. Pavarini, Phys. Rev. B **100**, 045116 (2019).
- <sup>11</sup> A. C. Komarek, H. Roth, M. Cwik, W. -D. Stein, J. Baier, M. Kriener, F. Bouree, T. Lorenz, and M. Braden, Phys. Rev. B 75, 224402 (2007).
- <sup>12</sup> M. Imada, A. Fujimori, and Y. Tokura, Rev. Mod. Phys. 70, 1039 (1998).
- <sup>13</sup> D.I. Khomskii, Transition Metal Compounds (Cambridge University Press, Cambridge, 2014).
- <sup>14</sup> M. Itoh, M. Tsuchiya, H. Tanaka, and K. Motoya, J. Phys. Soc. Jpn. **68**, 2783 (1999).
- <sup>15</sup> J. Akimitsu, H. Ichikawa, N. Eguchi, T. Miyano, M. Nishi, and K. Kakurai, J. Phys. Soc. Jpn. **70**, 3475 (2001).
- <sup>16</sup> H. Ichikawa, J. Akimitsu, M. Nishi, and K. Kakurai, Physica B: Cond. Matt. 281-282, 482 (2000).
- <sup>17</sup> M. Ito, N. Tuji, F. Itoh, H. Adachi, E. Arakawa, K. Namikawa, H. Nakao, Y. Murakami, Y. Taguchi, and Y. Tokura, J. Phys. Chem. Sol. **65**, 1993 (2004).

- <sup>18</sup> I. A. Kibalin, Z. Yan, A. B. Voufack, S. Gueddida, B. Gillon, A. Gukasov, F. Porcher, A. M. Bataille, F. Morini, N. Claiser *et al.*, Phys. Rev. B **96**, 054426 (2017).
- <sup>19</sup> H. Nakao, Y. Wakabayashi, T. Kiyama, Y. Murakami, M. v. Zimmermann, J. P. Hill, D. Gibbs, S. Ishihara, Y. Taguchi, and Y. Tokura, Phys. Rev. B 66, 184419 (2002).
- F. Iga, M. Tsubota, M. Sawada, H. B. Huang, S. Kura, M. Takemura, K. Yaji, M. Nagira, A. Kimura, T. Jo, T. Takabatake, H. Namatame, and M. Taniguchi, Phys. Rev. Lett. 93, 257207 (2004).
- <sup>21</sup> G. Khaliullin and S. Maekawa, Phys. Rev. Lett. **85**, 3950 (2000).
- M. Cwik, T. Lorenz, J. Baier, R. Müller, G. André, F. Bourée, F. Lichtenberg, A. Freimuth, R. Schmitz, E. Müller-Hartmann, and M. Braden, Phys. Rev. B 68, 060401(R) (2003).
- M.W. Haverkort, Z. Hu, A. Tanaka, G. Ghiringhelli, H. Roth, M. Cwik, T. Lorenz, C. Schüßler-Langeheine, S. V. Streltsov, A. S. Mylnikova, V. I. Anisimov, C. de Nadai, N. B. Brookes, H. H. Hsieh, H.-J. Lin, C. T. Chen, T. Mizokawa, Y. Taguchi, Y. Tokura, D. I. Khomskii, and L. H. Tjeng, Phys. Rev. Lett. 94, 056401 (2005).
- <sup>24</sup> T. Kiyama and M. Itoh, Phys. Rev. Lett. **91**, 167202 (2003).
- <sup>25</sup> M. Mochizuki and M. Imada, Phys. Rev. Lett. **91**, 167203 (2003).
- <sup>26</sup> P. Lunkenheimer, T.Rudolf, J. Hemberger, A. Pimenov, S. Tachos, F. Lichtenberg, A. Loidl, Phys. Rev. B 68, 245108 (2003).
- <sup>27</sup> M. Mochizuki and M. Imada, J. Phys. Soc. Jap. **70**, 1777 (2001); J. Phys. Soc. Jap. **70**, 2872 (2001).
- <sup>28</sup> M. Mochizuki and M. Imada, J. Phys. Soc. Jap. **73**, 1833 (2004).
- <sup>29</sup> D. A. Maclean, H.-N. Ng, and J. E. Greedan, J. Sol. Stat. Chem. **30**, 35 (1979).
- <sup>30</sup> P. Blaha, K. Schwarz, P. Sorantin, and S. Trickey, Comp.

- Phys. Comm. **59**, 399 (1990).
- <sup>31</sup> N. Marzari and D. Vanderbilt, Phys. Rev. B **56**, 12847 (1997).
- <sup>32</sup> T. Mizokawa and A. Fujimori, Phys. Rev. B **54**, 5368 (1996).
- E. Gull, A. J. Millis, A. I. Lichtenstein, A. N. Rubtsov, M. Troyer, and P. Werner, Rev. Mod. Phys. 83, 349 (2011).
- <sup>34</sup> M. Mochizuki and M. Imada, New J. of Phys. 6, 154 (2004).
- <sup>35</sup> A.M. Oleś, G. Khaliullin, P. Horsch, L.F. Feiner, Phys. Rev. B **72**, 214431 (2005).
- <sup>36</sup> A.M. Oleś, in E. Pavarini, E. Koch, R. Scalettar, and R. M. Martin (eds.) The Physics of Correlated Insulators, Met-

- als, and Superconductors Modeling and Simulation, Vol. 7 (Verlag des Forschungszentrum Jülich, Jülich, 2017); A.M. Oleś, Acta Physica Polonica A 118, 212 (2010).
- <sup>37</sup> A. B. Harris, T. Yildirim, A. Aharony, O. Entin-Wohlman, and I. Ya. Korenblit, Phys. Rev. Lett. **91**, 087206 (2003); Phys. Rev. B **69**, 035107 (2004).
- <sup>38</sup> M. Mochizuki and M. Imada, J. Phys. Soc. Jap. **69**, 1982 (2000).
- Notice that in Refs. 15,16,18,20 the local z axis is in the direction of the longest Ti-O bond. This differs from the convention adopted in this work (see caption of Fig. 1).